Beyond the Born-Oppenheimer static surface model for molecule-surface reactions

Spiering, P.

Chapter 5

Orbital-Dependent Electronic Friction Significantly Affects the Description of Reactive Scattering of N_2 from Ru(0001)

This chapter is based on P. Spiering et al. "Orbital-Dependent Electronic Friction Significantly Affects the Description of Reactive Scattering of N_2 from Ru(0001)". In: *J. Phys. Chem. Lett.* 10 (2019), pp. 2957–2962.

Abstract

Electron-hole pair (ehp) excitation is thought to substantially affect the dynamics of molecules on metal surfaces, but it is not clear whether this can be better addressed by orbital dependent friction (ODF) or the local density friction approximation (LDFA). This chapter discusses the effect of ehp excitation on the dissociative chemisorption of N_2 on and its inelastic scattering from Ru(0001), which is the benchmark system of highly activated dissociation, with these two rivaling models. ODF yields results for sticking, energy transfer to the surface and vibrational excitation of N_2 that are in significantly better agreement with existing experimental data than the LDFA results. N_2 on Ru(0001) is thus the first system for which the ODF and LDFA approaches are shown to yield substantially different results for easily accessible experimental observables including reaction probabilities, making it a good test system for modeling ehp excitation for reactive scattering.

5.1 Introduction

In the dawning age of sustainability, chemical reactions on metal surfaces play a crucial role in heterogeneously catalysed processes that feed and fuel our modern societies. The corresponding reaction rates are usually obtained based on the Born-Oppenheimer (BO) approximation and concomitant (adiabatic) potential energy surfaces (PESs) [2, 3]. It has been suggested that non-adiabatic effects in the form of ehp excitations, which are not captured within the BO approximation, may significantly affect the underlying dynamics of molecules on metal surfaces [4–10]. However, non-adiabatic effects cannot be quantified by experimental data alone. Instead, state-of-the-art first-principles based computer simulations are mandatory, in combination with measurements from well-defined molecular beam experiments under clean ultra-high vacuum conditions.

The current workhorse model for including non-adiabatic effects in simulations of molecular beam experiments is molecular dynamics with electronic friction (MDEF) [11, 12], with two rivaling theoretical approaches for obtaining the electronic friction coefficients: The local density friction approximation (LDFA) determines the latter

based on the surface electron density [13] according to the computationally inexpensive atoms-in-jellium model [14].

The LDFA enables the inclusion of all degrees of freedom of a molecule in dynamical simulations[13, 15], but at the same time implies the independent atom approximation (IAA) in most practical applications, thus neglecting any potential molecular effects [16, 17]. This is no problem for atomic projectiles, and the LDFA yields accurate results for atoms scattering from metal surfaces [18]. Orbital-dependent friction (ODF) invokes first order time-dependent perturbation theory for the Kohn-Sham orbitals resulting from density functional theory calculations of an atom or molecule interacting with the surface [11, 12, 19], so that the effects of molecular electronic structure are taken into account (no IAA). ODF is thus expected to be important for reactive scattering of molecules from metal surfaces [16, 20–22]. However, recently, the pragmatic use of broadening techniques for the calculation of ODF coefficients, which is currently without any alternative [19, 20, 22–24], has been criticized to affect the values obtained for these coefficients in an undefined fashion [25]. In summary, the LDFA and ODF as now implemented both have advantages and disadvantages, and a clear verification is still pending for which of the two methods best describes dissociative chemisorption. Due to the very high computational cost of ODF it has only recently been used for the simulation of reactive scattering in two systems, i.e., H_2 and D_2 from Ag(111) [22, 24] and Cu(111) [23], including all six molecular degrees of freedom. For these two system no significant differences were found between reaction probabilities computed with ODF and the LDFA.

Given this situation, other systems are required that offer the possibility to distinguish LDFA and ODF, ideally by benchmarking against data from molecular beam experiments. Luntz and coworkers have suggested that N_2 on Ru(0001) could be such a system after extensive experimental and pioneering low-dimensional computational studies [26–28]. This prototypical case of highly activated diatomic molecule dissociation has received much attention due to the relevance of N_2 dissociation as rate-limiting step for ammonia production via the Haber-Bosch process[29]. Recent results from LDFA calculations indicate that electronic friction is not important for the dissocia-

tive chemisorption probability [30], whereas experiments have demonstrated that N_2 molecules associatively desorbing from Ru(0001) experience a large amount of vibrational quenching[31, 32] that cannot be explained using BO-based theory[26, 33].

This chapter shows that the high-dimensional ODF model [23] already presented in Chap. 4 but now applied to N_2 on Ru(0001), which includes frictional couplings and the motion in all six molecular degrees of freedom, reduces the dissociative chemisorption probability by about 50% compared to both adiabatic calculations and the LDFA. Furthermore, the results in this chapter demonstrate that ODF improves the description of energy transfer during scattering and provides the best agreement with the corresponding experimental data. N_2 on Ru(0001) is thus the first system for which the ODF and LDFA approaches are shown to yield substantially different results for easily accessible experimental observables including reaction probabilities. The error bars of the experimental data still prevent an unequivocal verification of the quantitative performance of ODF. Nevertheless, our results pave the way for subsequent improved experimental and theoretical studies which will clearly show whether ODF indeed better describes the non-adiabatic reaction in this benchmark system, as our present calculations suggest.

5.2 Methods

MDEF [11, 12] calculations are performed according to the generalized Langevin equation (GLE)

$$m_i \frac{d^2\mathbf{r}}{dt} = -\nabla V\left(\mathbf{r}^{N_2}, \mathbf{r}^{Ru}\right) \; - \; \sum \boldsymbol{\eta}^{N_2}\left(\mathbf{r}^{N_2}\right) \frac{\mathbf{dr}^{N_2}}{dt} \; + \; \mathcal{F}^{N_2}\left(\boldsymbol{\eta}, T_s\right) \quad , \tag{5.1}$$

where $V\left(\mathbf{r}^{N_2}, \mathbf{r}^{Ru}\right)$ is the potential energy surface that describes the (electronically adiabatic) interaction between a N_2 molecule and the Ru(0001) surface consisting of mobile surface atoms described by coordinates $\mathbf{r}^{N_2}$ and $\mathbf{r}^{Ru}$, respectively. The high-dimensional neural network (HD-NNP) PES from Shakouri et al. [34], which has been fitted to a DFT reference dataset based on the RPBE functional [35] using the Behler-Parinello method [36], is used for the potential energy surface and concomitant forces.

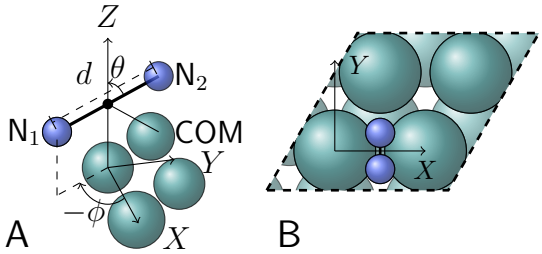

Figure 5.1: (A) Six-dimensional coordinate system for the description of N_2 molecules on Ru(0001), consisting of the center of mass (COM) coordinates (X,Y,Z) and the N_2 bond distance d as well as the polar angle θ and azimuthal angle ϕ. X,Y,Z = 0 corresponds to the position of a Ru atom in the surface plane (top site). (B) Top view of a N_2 molecule with its molecular axis parallel to the surface over a bridge site in a bridge-to-hollow orientation ($X = \frac{1}{2}a, Y = 0$, $\theta = 90°, \phi = 90°$). a denotes the surface lattice constant. First (second) layer Ru atoms are shown in (transparent) green. Dashed black lines show the periodic boundary conditions of a 2x2 super cell.

The friction tensor $\boldsymbol{\eta}^{N_2}$ and the random forces $\mathcal{F}^{N_2}$ $(\boldsymbol{\eta}, T_s)$ describe the non-adiabatic coupling of the N_2 molecules with electron-hole pair excitations in the surface at the surface temperature T_s. The ODF tensor [23] is calculated in the same way as in Chap. 4 from Density Functional Perturbation Theory. This 6×6 tensor depends on the six coordinates of the two nitrogen atoms, which are most conveniently described in the coordinate system shown in Figure 5.1. Subsequently, we have constructed an accurate continuous representation using a neural network approach as detailed in the supporting information, which – together with the HD-NNP PES – allows calculating a large enough number of trajectories to obtain sticking probabilities that can be compared to experimental data [34, 37]. Previous work has shown that surface atom displacements hardly affect the results of ab initio MDEF calculations based on the LDFA for N_2 on Fe(110) [38]. Therefore, the influence of surface atom displacements on the friction tensor is neglected for the results in this chapter.

In order to numerically integrate equation 5.1, I have adapted a recently suggested Liouville operator technique, denoted by OVRVO in ref [39], which simplifies to the

conventional velocity-Verlet algorithm[40] in the absence of friction. This technique allows defining a conserved total energy [41], which has enabled us to monitor and thus ensure the accuracy of the numerical integration of the trajectories. It has also greatly simplified the analysis of the energy exchange with the surface – in particular for the non-adiabatic energy which is dissipated into the electron-hole pair excitations in the surface.

First a comparison is made between the results obtained with the new ODF model and previous results using LDFA and adiabatic simulations for a mobile surface (BOMS) without electronic friction (i.e. without the last two terms in Eq. 5.1), focusing on a surface temperature $T_s = 575$ K, which is comparable to the experimental conditions for which data has been obtained [26, 27, 42] and relevant for catalytic conditions of the Haber-Bosch cycle. In more approximate calculations all the Ruthenium atoms are frozen at their equilibrium positions, resulting in the so-called Born-Oppenheimer static surface (BOSS) model, which does not allow for any energy exchange with the surface [37, 43].

5.3 Results

Figure 5.2 shows the initial sticking probabilities for the dissociative chemisorption of N_2 on Ru(0001). Except for the lowest incidence energy (1.50 eV) the BOSS model does not reproduce the experimental results [42]. Including surface motion (BOMS) reproduces the experiment within error bars as has already previously been shown [30, 34]. The LDFA does not yield any significant changes compared to the BOMS model. The closest agreement is found with experimental data when the ODF model is used to describe the electronic friction. The effect of the ODF is quantified on a linear scale in the inset of Figure 5.2, which shows the decrease of the reaction probability of both electronic friction models relative to the BOMS results. Also on this scale, the results from the LDFA and BOMS model are hardly distinguishable. ODF on the other hand decreases the sticking probability, relative to BOMS, from lower to higher incidence energies by 61% to 41%.

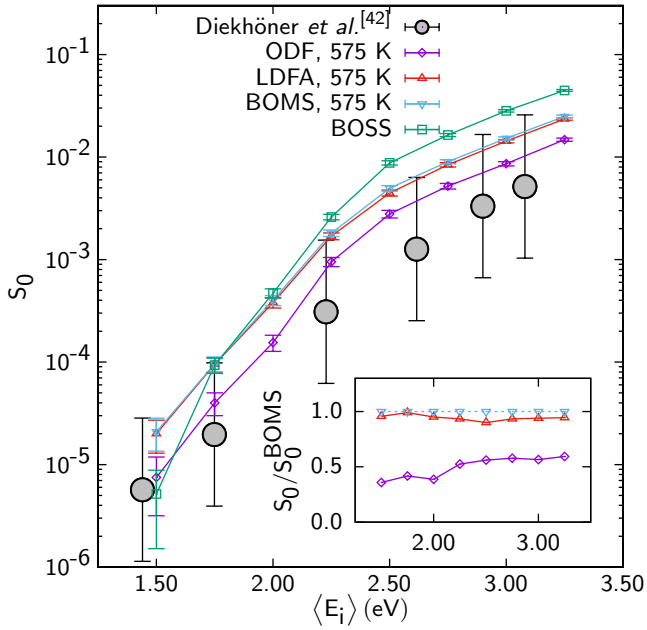

Figure 5.2: Reaction probability S_0 as a function of the average incidence energy $\langle E_i \rangle$ calculated with the ODF model from this work in combination with the HD-NNP potential energy surface [34] for a surface temperature $T_s = 575$ K (purple diamonds). Corresponding results from Shakouri et al. [30] based on the LDFA ($T_s = 575$ K, red triangles), adiabatic calculations for a mobile surface ($T_s = 575$ K) and a frozen surface, i.e. the BOMS (blue triangles) and the BOSS model (green squares). Experimental data from Diekhöner et al. [42] are shown for comparison (gray circles). The inset shows the ratio of reaction probabilities calculated with both electronic friction models relative to the corresponding adiabatic BOMS results.

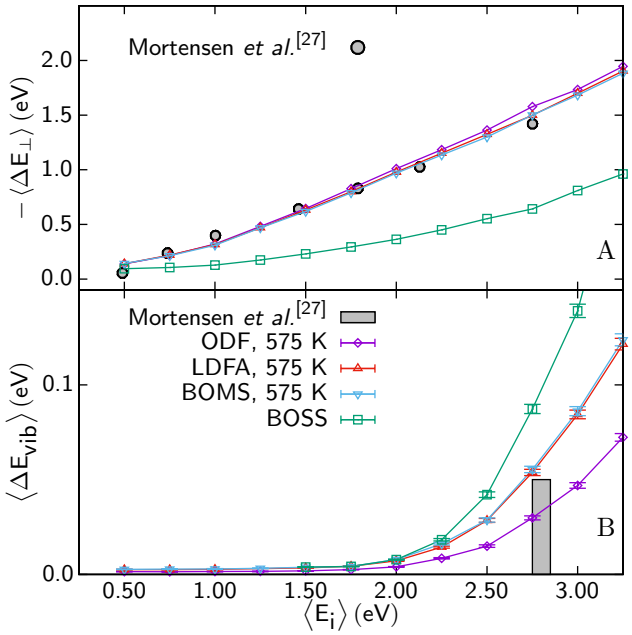

Figure 5.3: (A) Average energy uptake of the surface $\langle \Delta E_{\mathrm{surface}} \rangle$ and (B) average change of the vibrational energy $\langle \Delta E_{\mathrm{vib}} \rangle$ as a function of the average incidence energy $\langle E_{\mathrm{i}} \rangle$ for molecules scattered from the surface. Using the HD-NNP PES from Ref. [34], results from adiabatic calculations according to the BOSS model (green squares), which does not account for energy dissipation by the surface, and a moving surface (blue triangles) as well as LDFA (red triangles) and ODF (purple diamonds) for a surface temperature $T_{\mathrm{s}} = 575$ K are plotted. Experimental data from Mortensen et al. [27] (gray circles) are shown for comparison in (A). In (B), the maximum vibrational energy change of 0.05 eV at $\langle E_{\mathrm{i}} \rangle = 2.8$ eV estimated in the same study [27] is indicated (gray bar).

Analyzing the energy exchange for N_2 scattering from Ru(0001) provides further insights into the strong effect of ODF. Figure 5.3A shows the average energy uptake $\Delta E_{\mathrm{surface}}$ of the Ru(0001) surface for N_2 scattering at different incidence energies. The BOMS model already yields semi-quantitative agreement with the experimental data, with the non-adiabatic energy dissipation channel as described by LDFA only resulting in a minor increase of $\Delta E_{\mathrm{surface}}$ by 3-4%.[30] ODF on the other hand increases $\Delta E_{\mathrm{surface}}$ by 15-20%, such that the energy losses are significantly closer to the experimental data from Mortensen et al. [27] at high incidence energies. In the same experiments, an upper bound of 0.05 eV has been obtained for the amount of vibrational excitation during N_2 scattering from Ru(0001) at $\langle E_{\mathrm{i}} \rangle = 2.8$ eV. Earlier calculations within the BOSS model [43] using a different RPBE-based PES[37] have significantly overestimated this energy transfer $\langle \Delta E_{\mathrm{vib}} \rangle$. As shown in Figure 5.3B, the new results reproduce this finding for BOSS-model-based simulations with the HD-NNP PES . Including surface mobility (BOMS) reduces the average vibrational excitation up to 50% at the highest incidence energies, but the results are not yet compatible with the upper bound estimated from the experiments. LDFA does not yield any further improvement. Quite in contrast, ODF leads to a further reduction of 50-60% for all incidence energies, such that only this electronic friction model is compatible with the experimental upper bound.

The big effect of ODF on the S_0 and the energy exchange of scattered molecules with the surface is due to the extremely large electronic friction acting on the motion towards the surface, along the N_2 bond axis as well as the strong coupling between the two, the latter of which is absent with the LDFA. Figures 5.4A-C show the corresponding friction elements η_{ZZ}, η_{dd} and η_{dZ}, respectively, along the minimum energy path q obtained by Shakouri et al. [30] for the HD-NNP PES used in this chapter. The ODF tensor elements for N_2 on Ru(0001) are more than five times larger than for H_2 on Cu(111) [23]. Furthermore, as has been observed before [16, 22, 23, 28], ODF predicts an increased friction along η_{dd} compared to LDFA, i.e. $\eta^{\mathrm{ODF}}{}_{dd} > 10\,\eta^{\mathrm{LDFA}}_{dd}$ in contrast to $\eta^{\mathrm{ODF}}_{ZZ} \approx 4\,\eta^{\mathrm{LDFA}}_{ZZ}$ at the transition state. Hence it is not surprising that any dynamics that involves N_2 bond activation, like dissociation on and inelastic scattering from the Ru(0001) surface, experiences a significantly larger concomitant

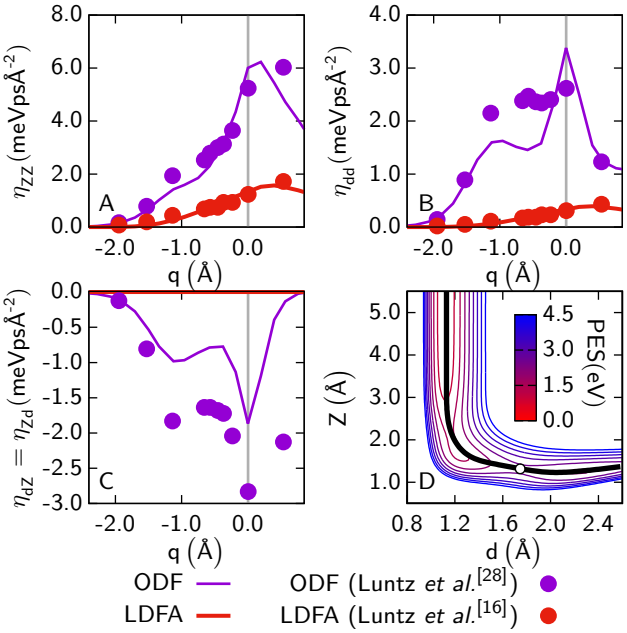

Figure 5.4: (A-C) Friction tensor elements related to the center of mass distance to the surface (η_{ZZ}), the bond length (η_{dd}) and the friction-induced coupling between these two (η_{dZ}), respectively, along the minimum energy path q for dissociative chemisorption over the bridge site in the bridge-to-hollow orientation with the molecular axis slightly tilted off parallel from the surface ($\theta = 84°$, see Figure 5.1 for the molecular coordinate system). This path is depicted in (D) together with the corresponding two-dimensional PES cut. The purple (red) lines indicate the electronic friction obtained for ODF (LDFA). Purple (red) dots show the ODF (LDFA) results from previous work of Luntz and Persson [16, 28]. The transition state for dissociation is located at the vertical gray line in (A-C) ($q = 0$ Å) and indicated by the empty circle in (D). Negative numbers up to transition state denote the approach from the gas-phase (i.e. decreasing Z above the surface). It should be noted that in Ref. [28] q is defined for the strictly parallel approach of the N_2 molecule towards the surface ($\theta = 90°$), but this does not correspond to the minimum energy path in our HD-NNP PES [30].

non-adiabatic energy loss with ODF than with LDFA. Luntz and Persson have already pointed out large differences between ODF and LDFA [16], but the dynamical model in their pioneering work only included two degrees of freedom of the N_2 molecule (Z and d). Our results for η_{ZZ}, η_{dd} and η_{dZ} slightly differ from theirs, but still maintain the same essential features that distinguish LDFA from ODF. In Sec. 5.C it is shown that these differences are related to a slightly different minimum energy path and the use of a different exchange-correlation functional.

5.4 Conclusion

In conclusion, for N_2 on Ru(0001), the new ODF approach, which includes non-adiabatic coupling of the motion in all six N_2 molecular degrees of freedom due to ehp excitations, yields a reduction of the dissociative chemisorption probability by about 50%. Such a large effect on a reaction probability has never been observed for MDEF calculations before, most of which have been based on the rivaling LDFA model. ODF agrees best with the best experimental estimates of S_0, but ODF and LDFA both agree within current error bars. ODF yields results for the energy transfer to the surface and vibrational excitation that are in significantly better agreement with the aforementioned experiments than the LDFA. Consequently, more accurate measurements of the reaction probabilities would allow to further develop theoretical modeling of non-adiabatic dynamics at metal surfaces – for example by including higher order perturbation terms (electron-mediated phonon-phonon coupling), which Novko et al. demonstrated to play a crucial role for the non-adiabatic vibrational damping of CO on Cu(100) [25, 44, 45]. Likewise, improvements of the exchange-correlation functional defining the PES might be required in order to achieve quantitative agreement [46, 47] with the more accurate experimental data to be measured. Given the importance of this system as a prototypical case of highly activated dissociative chemisorption, this would be an important step towards understanding whether and how non-adiabatic effects need to be accounted for in heterogeneous catalysis.

5.5 Computational Details

The orbital dependent electronic friction tensors have been obtained from density functional perturbation theory (DFPT)[48] results based on a computational setup similar to that in Chap. 4, which was used for H_2 on Cu(111) [23]. Briefly, DFPT calculations are performed as implemented in the Quantum Espresso package[49] for a 2x2 Ru(0001) slab with 5 layers employing the RPBE functional[35] as implemented in LibXC[50]. Using ONCV[51] pseudopotentials from the SG15[52] library together with a plane-wave cutoff of 816eV, a 18x18x1 k-point grid and a Gaussian envelope technique with a width of 0.6 eV for the sum over electronic states [19, 25] yields converged results for the friction tensor elements. A continuous representation of the 6x6 frozen-surface friction tensor was obtained using neural networks constructed with the help of the TensorFlow package[53]. Improving our previous approach[23], special care has been taken in order to ensure positive definiteness of the friction tensor and to keep the amount of neural network weight parameters as small as possible (3 hidden layers with 20 nodes each) by fitting all 21 independent friction tensor elements simultaneously.

Quasi-classical trajectory calculations with a time step of 0.3 fs were performed using the LAMMPS package [54], into which I have implemented an adaptation of the OVRVO algorithm [39]. At every time step, the OVRVO is applied by rotating to the six-dimensional coordinate system in which the ODF tensor is diagonal. The diagonal LDFA friction tensor is the same as in Ref. [30] and this new OVRVO implementation perfectly reproduces the results from that work. Likewise, the same equilibration procedure of the surface slab for generating initial conditions at $T_s > 0$ K is used.

5.A Additional Details on Dynamical Simulations

In the quasi-classical trajectory calculations, the incident velocity is Monte Carlo sampled from a flux-weighted velocity distribution describing the beams used in the experiments of Diekhöner et al. [42] as described in refs [30, 34]. Likewise, the other initial conditions are Monte Carlo sampled as described in ref [30]. Initial sticking probabilities S_0 are obtained by counting the number of trajectories that ended with

a N-N distance larger than 2.7 Å (i.e. more than 2.5 times the equilibrium distance in gas phase) and dividing it by the total number of trajectories. Trajectories are stopped and counted as scattered when N_2 molecules are reflected to distances more than 6 Å away from the surface. Like in Chap. 4, they are assigned a final rovibrational state by binning first to the closest allowed angular momentum J while observing a $\Delta J = \text{even}$ selection rule, and second to the closest rovibrational energy with the previously obtained angular momentum, which is based on solving the 1-dimensional Schrödinger equation of the molecule in gas phase including rotational effects [23].

Consistent with previous calculations [43] and the analysis of the experiments [27], the average vibrational energy change is computed within the quasi-classical trajectory simulations according to

$$\langle \Delta E_{\text{vib}} \rangle (E_{\text{i}}) = \sum_{\nu_{\text{f}}} P_{\nu_{\text{f}}}(E_{\text{i}}) \cdot (E_{\nu_{\text{f}}} - E_0) \tag{5.2}$$

where $P_{\nu_{\text{f}}}(E_{\text{i}})$ is the probability of finding a scattered N_2 molecule with the initial vibrational state $\nu_{\text{i}} = 0$ in the final rovibrational state $\nu_{\text{f}} > 0$ and $J_{\text{f}} \leq 13$ at incidence energy E_{i}. In order to disentangle rotational and vibrational energy, the vibrational excitation energy of a non-rotating N_2 molecule $E_{\nu_{\text{f}}} - E_0$ is used, resulting from the quantum mechanical solution of the effectively one-dimensional part of the HD-NNP PES at molecule surface distance larger than 10 Å.

5.B Continuous Representation of the Orbital-Dependent Friction Tensor

5.B.1 Choice of Reference Angles θ_0 and ϕ_0

The same 4D+2D model [23] was used as in Chap. 4, with the same reference angles $\theta_0 = 90°$ and $\phi_0 = 90°$. Here the continuous representation of the 6x6 cartesian friction tensor depending on all 6 N_2 coordinates (see Fig.5.1), is constructed according to

$$\eta^{\text{N}_2}(\mathbf{R}) \approx T(\theta, \phi) \eta^{\text{N}_2}(X, Y, Z, d) T^{-1}(\theta, \phi), \tag{5.3}$$

where $T(\theta, \phi)$ is the appropriate rotation matrix and $\eta^{N_2}(X, Y, Z, d)$ is a 4D continuous neural network representation based on the center of mass coordinates of N_2 together with the bond distance using symmetry adapted coordinates [55, 56]. This ensures that our neural network representation yields a symmetry-compliant friction tensor.

Reactive trajectories

The angular distributions for reacted molecules (Figures 6a and 6b from Ref. [30]) show that the majority of the reactive trajectories follow the $\theta \approx 90°$ (or symmetrically equivalent orientation) and $\phi \approx 90°$ bridge reaction path. This is not surprising as this reaction path has by far the lowest barrier. Since the reaction probability is dominated by N_2 molecules approaching the surface at the chosen reference θ and ϕ, it is expected that this model works well for computing the reaction probabilities. Even though the argument here is that most reacted trajectories are at $\theta \approx 90°$ and $\phi \approx 90°$, for those that do not, the same argument as for the scattered trajectories, which are presented in the next section, can be used.

Scattered trajectories

Scattered trajectories are not limited to a $\theta \approx 90°$ and $\phi \approx 90°$ approach, however, the 4D+2D model is still appropriate using the following arguments. First of all, the difference in the magnitude between LDFA friction and ODF along the reaction path q as presented in Figure 5.4 is much larger than the differences between ODF at different orientations along q. We thus conclude that the large difference between LDFA and our isotropic ODF model will remain at least qualitatively.

In order to estimate the effect of the 4D+2D model on the dynamics, the friction element η_{dd} direction is considered for different orientations of N_2 along the reaction path in Figure 5.5 and 5.6 for rotated θ and ϕ respectively. Figure 5.5b shows the potential along the reaction path for different orientations along θ. Only at $\theta = 90°$ is a surmountable barrier present at q=0 Å while at other orientations the potential is essentially a repulsive wall. This means that N_2 molecules scattering from the surface at orientations different from $\theta = 90°$ do not approach the surface as closely and at

the same distance from the surface they will generally have a smaller velocity because of a repulsive force created by the potential. Since the energy dissipation rate, while neglecting the contribution from random forces, $\dot{E}_{\mathsf{diss}}^{\mathrm{N_2}}$ of N_2 at time t during a trajectory is proportional with the square of the velocity $\mathbf{v}^{\mathrm{N_2}}$ according to

$$\dot{E}_{\mathsf{diss}} = \mathbf{v}^{\mathrm{N_2}}(t)\boldsymbol{\eta}^{\mathrm{N_2}}(t)\mathbf{v}^{\mathrm{N_2}}(t), \tag{5.4}$$

the energy loss for trajectories at different orientations than $\theta = 90°$ must be smaller and thus non-adiabatic effects are less important for those trajectories. When considering the friction tensor itself in Figure 5.5a, it can be seen that at orientations different from $\theta = 90°$ (using dashed lines) the friction tensor itself is smaller at least until the closest possible approach, for the largest incidence energy considered here, indicated by the gray dashed line.

For the anisotropy of η_{dd} for rotations along ϕ (Figure 5.6) essentially the same result as for Fig. 5.5 is found. At $\phi = 45°$ and $135°$, which are essentially identical, there is a barrier at q=0.25 Å, although it is not dynamically accessible. The closest approach for orientations different from $\phi = 90°$ is closer to the transition state compared to θ and is 0.1 Å before the $\phi = 90°$ barrier. While at very close approaches the friction tensor in Figure 5.6 is higher for the $\phi = 90°$ orientation, the overall energy loss will still be an underestimation due to the friction being much lower for $\mathsf{q} < -0.3$ Å. Consequently, the 4D+2D model, which uses slightly smaller values for both $\theta = 90°$ and $\phi = 90°$ in all cases, underestimates the amount of friction and dissipated energy. Since the current model already reports a much larger effect of friction for ODF compared to LDFA, this underestimation would not change any of the conclusions and in fact, the non-adiabatic effects on the observables may be even (slightly) larger for this system than predicted.

5.B.2 Neural Network Fitting Accuracy

In this section the neural network (NN) fitting accuracy of the orbital dependent friction (ODF) elements is assessed. In contrast to the fitting procedure in Chap. 4 and the work by Jiang and coworkers [24], the friction elements independently [23] are not fitted

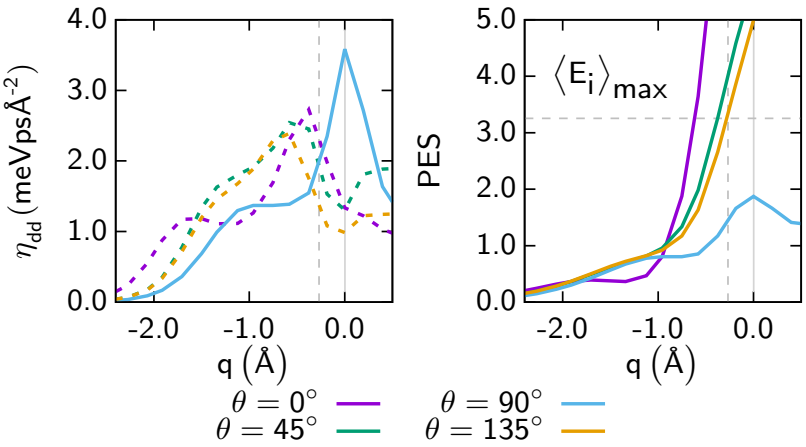

Figure 5.5: a) ODF along the reaction path for $\phi = 90°$, $X = \frac{1}{2}a$, $Y = 0$, and $\theta = 0°$ (purple), 45° (green), 90° (blue), 135° (orange). Orientations different from the reference rotation $\theta = 90°$ are shown using dashed lines since they are not included in the 4D+2D model. See Fig. 5.1 for the coordinate system. b) The potential energy is shown along the same reaction paths as in a). The vertical solid gray line is positioned at the barrier. The horizontal and vertical dashed gray lines indicate the largest $\langle E_i \rangle$ used in molecular dynamics simulations and the corresponding closest approach to the barrier, respectively, when $\theta \neq 90°$.

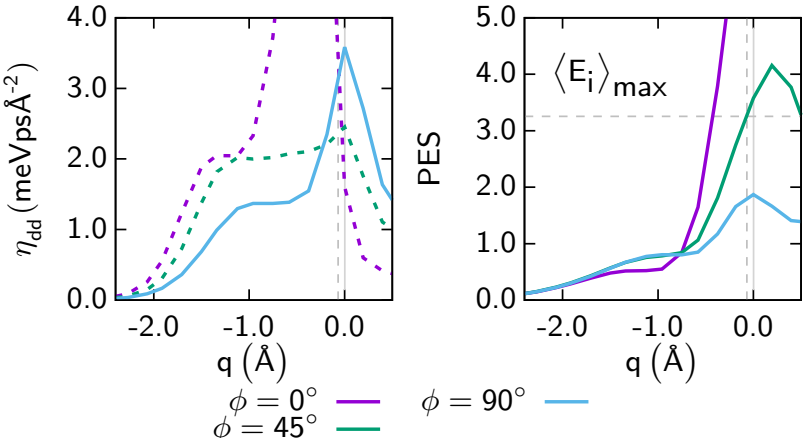

Figure 5.6: ODF along the reaction path for $\theta = 90°$, $X = \frac{1}{2}a$, $Y = 0$, and $\phi = 0°$ (purple), 45° (green), 90° (blue). Orientations away from the reference rotation $\phi = 90°$ are shown using dashed lines since they are not included in our isotropic friction model. See Fig.5.1 for the coordinate system. b) The potential energy is shown along the same reaction paths as in a). The vertical solid gray line is positioned at the barrier. The horizontal and vertical dashed gray lines indicate the largest $\langle E_i \rangle$ used in molecular dynamics simulations and the corresponding closest approach to the barrier, respectively, when $\phi \neq 90°$.

independently. Instead a single NN is used to fit all 21 independent friction elements simultaneously. To do this, 3 hidden layers ($N_{\mathsf{HL}} = 3$) and 20 nodes ($N_{\mathsf{HN}_i} = 20$) are used for each layer i together with an output layer of 21 nodes (N_{ON}). Subsequently, these 21 output nodes are arranged in the form of a lower triangular matrix. This ensures that a positive definite matrix is obtained as is required for finite temperature Langevin dynamics. A detailed discussion of the advantages of this approach will be the subject of a forthcoming publication. This construct is fitted using TensorFlow [53] to the friction elements obtained from DFPT.

By fitting only a single NN instead of 21 NNs the amount of free parameters (weights and biases) to be optimized is greatly reduced. The number of free parameters is determined according to

$$N_{\mathsf{IN}} \cdot N_{\mathsf{HN}_1} + N_{\mathsf{HN}_1} + \sum_{i=1}^{N_{\mathsf{HL}}-1} \left(N_{\mathsf{HN}_i} \cdot N_{\mathsf{HN}_{i+1}} + N_{\mathsf{HN}_{i+1}} \right) + N_{\mathsf{HN}_{N_{\mathsf{HL}}}} \cdot N_{\mathsf{ON}} + N_{\mathsf{ON}}, \quad (5.5)$$

where N_{IN} is the number of (symmetry) input coordinates. Using 21 independent NNs with 2 hidden layers and 20 nodes a total of 21·961=20181 free parameters are obtained. Instead, when using a single NN with an additional hidden layer and 21 output nodes, only 1381 free parameters are required. Note that for each configuration of the molecule, 21 independent friction elements are obtained. It should be emphasized here that the additional third hidden layer is needed in order to fit all elements with a single NN. This method works because while the elements are indeed independent, their behavior with respect to the molecules degrees of freedom is similar.

Several NN fits (1 through 5) have been obtained for the ODF elements in order to assess possible under or overfitting, where the only difference is the random initialization of the free parameters. This is sometimes referred to as a NN committee [57, 58].

Fitting error In Figure 5.7 the fitting error is shown for all NN fits for both the test and train set. With friction tensors, however, it is not directly clear how to interpret the error. For example, when the fitted friction tensor is slightly rotated with respect to the DFPT friction tensor, the cartesian representation of the friction tensor may be

different by either a large or a small amount depending on the starting rotation and specific values of the friction elements. The error of the train set is for all fits similar, while there are some slight differences in the error of the test set, which suggests a slight overfitting. For fit 1 in Figure 5.7A there are some larger test errors from 0.5 to 4.0 meVpsÅ^{-2}. On the other hand, fit 2 in Figure 5.7B has larger test errors above the diagonal at negative friction and below the diagonal at positive friction. The other fits are very similar and have errors distributed approximately symmetrically around the diagonal.

Fitting error along the reaction path In Fig. 5.8 a comparison is made for NN fits 1 and 5. Fig. 5.8 is the same as Fig. 5.4 and shows the result of two different fits in long and short dashed. For the friction elements η_{ZZ} and η_{dZ}, both neural networks predict the same result and are very close to the DFPT data. There is, however, a small discrepancy between both fits and the DFPT data 1Å before the barrier. Note that the points along the reaction path have not explicitly been included in the fitting data.

Dynamics for different neural network fits Performing molecular dynamics with electronic friction using different NN fits for ODF exposes the actual error introduced to observables due to the above mentioned fitting errors. Figure 5.9 shows that dynamics performed for both fit 1 and fit 5 are within one standard error of each other for all computed incidence energies. Fit 1 (long dash) was used for all other presented dynamics of ODF.

Concluding remarks From the dynamics performed on different fits in Figure 5.9 it is known that the errors reported here are small enough to obtain accurate dynamical observables for the N_2 on Ru(0001) system. Considering the different behavior of the test errors and the small influence on the dynamics, this amount of overfitting is negligible.

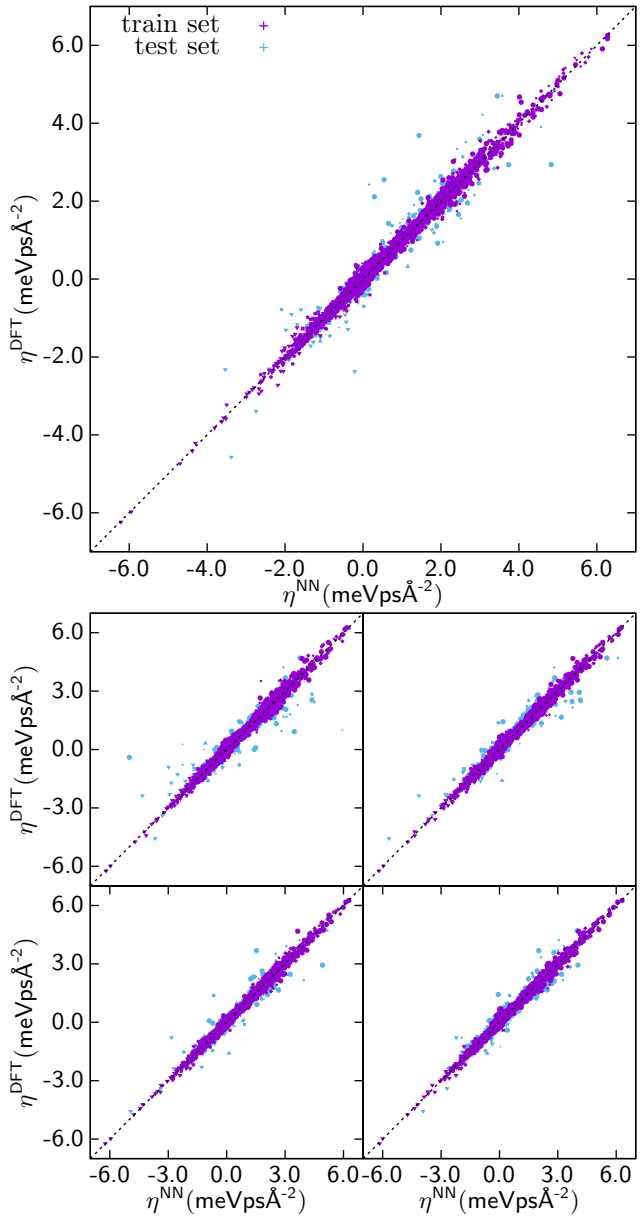

Figure 5.7: A-E show the correlation between the cartesian friction elements as calculated from DFPT (η^{DFT}) and NN fit 1 through 5, where the only difference between the fits is a different random initialization for the weights and biases.

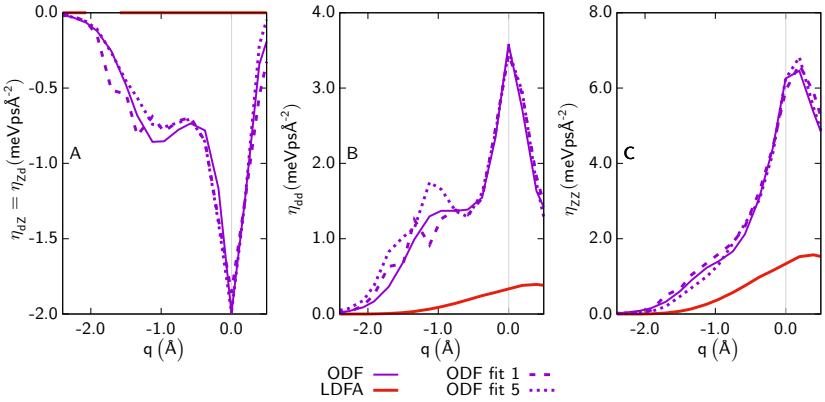

Figure 5.8: Same as Fig. 5.4. (A-C) show η_{dZ}, η_{dd} and η_{ZZ} in the molecular coordinate system, respectively, along the lowest minimum energy path for dissociative chemisorption over the bridge site (see Figure 5.1) for $\theta \approx 90°$ and $\phi \approx 90°$. ODF (solid-purple) and LDFA (solid-red) are from DFPT and DFT calculations respectively and are compared with fit 1 (long-dashed-purple) and fit 5 (short-dashed purple).

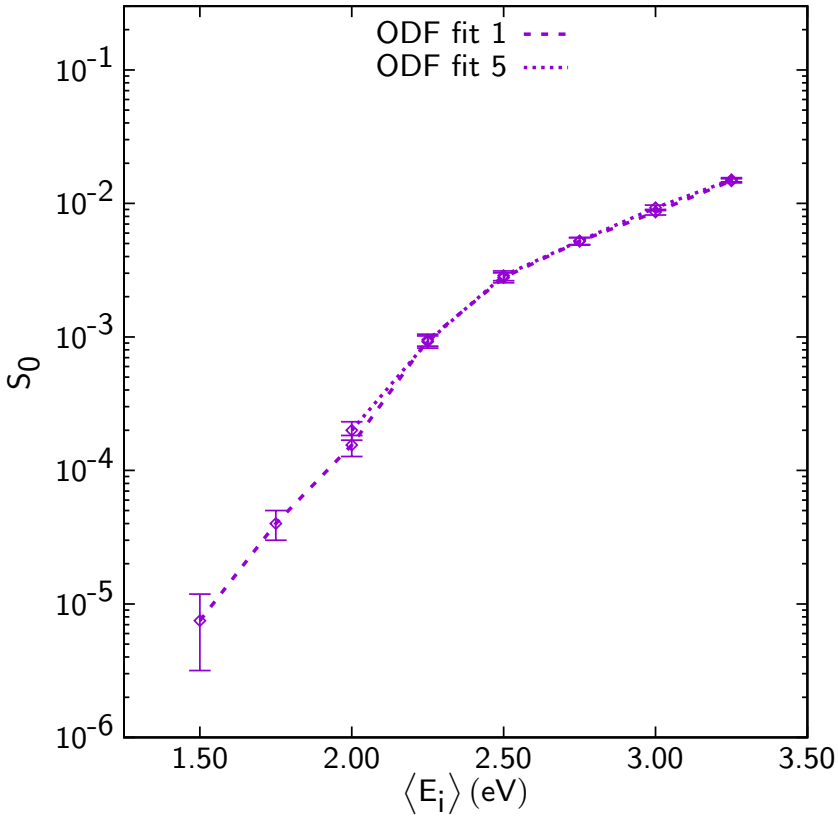

Figure 5.9: Same as Fig. 5.2. All calculated sticking probabilities are for surface atoms at a temperature of 575K. Results for fit 1 and 5 (see Figure 5.7) are in purple long dashed and short dashed respectively.

5.C Comparison with Previous Work

5.C.1 Low-Dimensional Orbital-Dependent Friction

In Fig. 5.4A it is illustrated that the results obtained for η_{ZZ} from Luntz et al. are very similar to the results presented earlier in this chapter along the reaction path. For η_{dd} in Figure 5.4B the same trend is seen in both cases; a peak is found at $q = 0$ together with a smaller peak at lower q. However, the friction from Luntz et al. is higher in front of the transition state while lower at the transition state. In section 5.B.1 it is found that for molecules that are rotated at the transition state that the peak at the transition state is lower. This may explain why Luntz et al. find a lower peak at the transition state as their minimum energy path is apparently not the lowest minimum energy path. The increased friction at lower q can also be due to differences in the treatment of the electronic structure.

Figure 5.4C shows a large difference in the magnitude of η_{dZ}, however, the shape is very similar. To obtain η_{dZ}, Luntz and Persson [28] have computed the friction along a different direction and applied a rotation to obtain the off-diagonal element. However, for the new results in this chapter η_{dZ} is obtained directly, which together with the different treatment of the electronic structure as well as the different reaction path may explain the difference in magnitude.

It seems that Luntz et al. [16] have obtained a different minimum energy path as they argue that the ratio of $\eta_{dd} : \eta_{ZZ}$ is 1:4 in the case of LDFA, which is not necessarily true if the polar angle $\theta \neq 90°$. Instead, Shakouri et al. [34] have found that the lowest minimum energy path is tilted by 6° with respect to the surface for which the elbow plot is shown in Fig. 5.4D together with the obtained lowest minimum energy path and transition state. Differences in the minimum energy path may further be explained due to a different treatment of the electronic structure.

Considering the comparison above, the argument is that at worst the new implementation has slightly underestimated the ODF, which would result in a smaller effect of electron-hole pairs and does not at all influence any of the conclusions drawn henceforth. The new LDFA coefficients are almost identical to those from Luntz et al. As

has been observed before, ODF predicts an increased friction along η_{dd} compared to LDFA since $\eta_{ZZ}^{\mathrm{ODF}} \approx 4\eta_{ZZ}^{\mathrm{LDFA}}$ while $\eta_{dd}^{ODF} > 10\eta_{dd}^{LDFA}$ at the transition state.

5.C.2 Ehrenfest Dynamics on Ruthenium Nanoclusters

It is interesting to also compare the new MDEF with ODF results with Ehrenfest dynamics of N_2 on Ruthenium nanoclusters by Montemore et al. [9]. They computed an effective increase of the barrier height by 70 meV due to non-adiabatic energy dissipation for a single trajectory on a Ru_{147}, starting with approximately 1.4 eV kinetic energy along the reaction path towards the transition state for dissociation. Despite all the differences between the initial conditions, the PESs for N_2 on a Ru_{147} cluster and the Ru(0001) surface as well as the underlying non-adiabatic dynamical propagation techniques and statistical averaging, the aforementioned 70 meV is in good agreement with the non-adiabatic contribution to $\langle \Delta E_{\mathrm{surface}} \rangle$ at $E_i \approx 1.4$ eV in Fig. 5.3A for the ODF simulations.

5.D Electronic Temperature Effects

Next the effect of the electronic temperature by performing calculations with (T_{el}=575K) and without (T_{el}=0K) random forces is discussed. In Fig. 5.10, the corresponding results are shown for the initial sticking probability. There is no qualitative difference in the resulting reaction probability, however, when random forces are neglected, the sticking probability is further reduced compared to simulations without electronic friction between an incidence energy of 2.0 and 3.25 eV. Neglecting random forces at lower incidence energies seem to increase this difference but I have not calculated a sufficient amount of trajectories in order to substantiate it beyond the statistical error bars.

In Fig. 5.11 a) and b) the same trend is observed that electronic friction at T_{el}=0K further increases the differences compared to simulations without electronic friction: the energy exchange with the surface in Figure 5.11 a) is slightly larger for T_{el}=0K. Surprisingly, the absolute difference with T_{el}=575K is independent from the incidence energy E_i between 1.5 eV and 3.25 eV and the shift is constant although small enough to not consider the random forces important for the energy exchange with the surface. The vibrational energy, however, is half at 2.25 eV and thus the random forces play an important role in the description of the vibrational quenching.

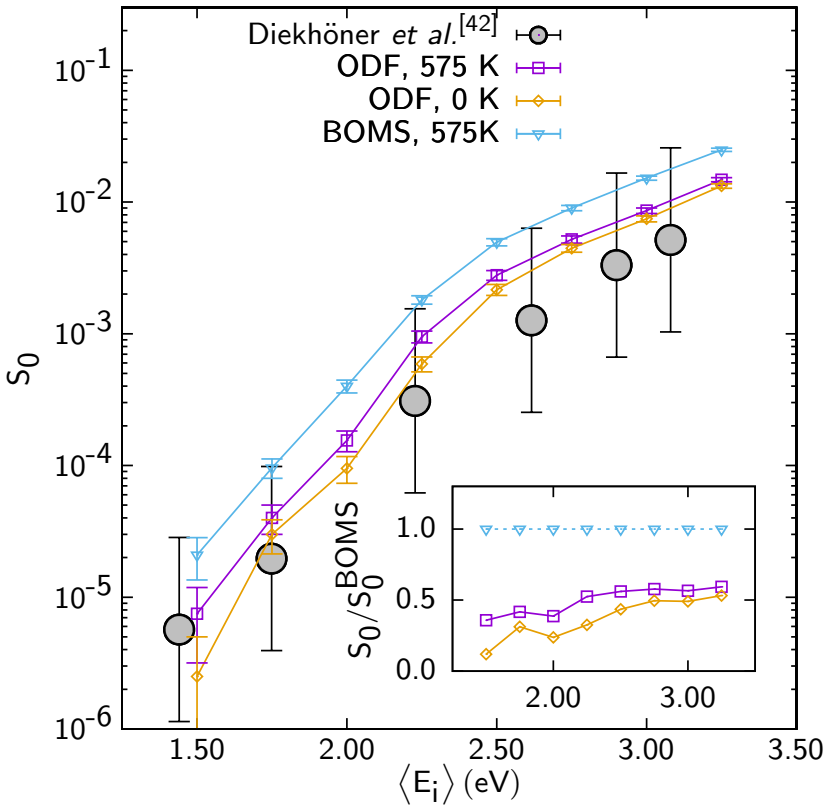

Figure 5.10: Same as Fig. 5.2. All calculated sticking probabilities are for surface atoms at a temperature of 575K. The "no friction" results (blue, BOMS previously in this chapter) is compared with ODF at an electronic temperature of 575K (purple, ODF previously in this chapter) and ODF at an electronic temperature of 0K (orange, neglecting random forces). Experimental sticking probabilities are the same as previously presented in this chapter. The inset shows the ratio of sticking probabilities with electronic friction turned on at T_{el} =0K and 575K with respect to the S_0 without friction

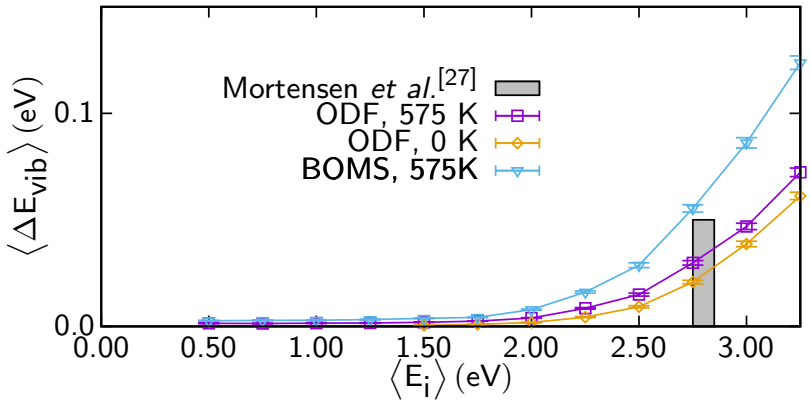

Figure 5.11: Same as Fig. 5.3. Both the energy exchange with the surface ($\langle \Delta E_{\text{surface}} \rangle$) and the vibrational excitation energy ($\langle \Delta E_{\text{vib}} \rangle$) have been obtained at a surface temperature of 575K The no friction results (blue, HD-NNP earlier in this chapter) is compared with HD-NNP+ODF at an electronic temperature of 575K (purple, HD-NNP+ODF earlier in this chapter) and HD-NNP+ODF at an electronic temperature of 0K (orange, neglecting random forces). Experimental energy exchanges and vibrational excitation energies are the same as earlier in this chapter.

References

[1] P. Spiering, K. Shakouri, J. Behler, G.-J. Kroes, and J. Meyer. "Orbital-Dependent Electronic Friction Significantly Affects the Description of Reactive Scattering of N_2 from Ru(0001)". In: *J. Phys. Chem. Lett.* 10 (2019), pp. 2957–2962. DOI: 10.1021/acs.jpclett.9b00523.

[2] K. Reuter. "First-Principles Kinetic Monte Carlo Simulations for Heterogeneous Catalysis: Concepts, Status, and Frontiers". In: *Modeling and Simulation of Heterogeneous Catalytic Reactions*. John Wiley & Sons, Ltd, 2011, pp. 71–111. DOI: 10.1002/9783527639878.ch3.

[3] K. Reuter. "Ab Initio Thermodynamics and First-Principles Microkinetics for Surface Catalysis". In: *Catal. Lett.* 146 (2016), pp. 541–563. DOI: 10.1007/s10562-015-1684-3.

[4] J. D. White, J. Chen, D. Matsiev, D. J. Auerbach, and A. M. Wodtke. "Conversion of Large-Amplitude Vibration to Electron Excitation at a Metal Surface". In: *Nature* 433 (2005), pp. 503–505. DOI: 10.1038/nature03213.

[5] M. Dell'Angela, T. Anniyev, M. Beye, R. Coffee, A. Föhlisch, et al. "Real-Time Observation of Surface Bond Breaking with an X-Ray Laser". In: *Science* 339 (2013), pp. 1302–1305. DOI: 10.1126/science.1231711.

[6] H. Öström, H. Öberg, H. Xin, J. LaRue, M. Beye, et al. "Probing the Transition State Region in Catalytic CO Oxidation on Ru". In: *Science* 347 (2015), pp. 978–982. DOI: 10.1126/science.1261747.

[7] D. Diesing and E. Hasselbrink. "Chemical Energy Dissipation at Surfaces under UHV and High Pressure Conditions Studied Using Metal–Insulator–Metal and Similar Devices". In: *Chem. Soc. Rev.* 45 (2016), pp. 3747–3755. DOI: 10.1039/C5CS00932D.

[8] A. M. Wodtke. "Electronically Non-Adiabatic Influences in Surface Chemistry and Dynamics". In: *Chem. Soc. Rev.* 45 (2016), pp. 3641–3657. DOI: 10.1039/C6CS00078A.

[9] M. M. Montemore, R. Hoyt, G. Kolesov, and E. Kaxiras. "Reaction-Induced Excitations and Their Effect on Surface Chemistry". In: *ACS Catal.* 8 (2018), pp. 10358–10363. DOI: 10.1021/acscatal.8b03266.

[10] A. Peña-Torres, H. F. Busnengo, J. I. Juaristi, P. Larregaray, and C. Crespos. "Energy Dissipation Effects on the Adsorption Dynamics of N2 on W(100)". In: *J. Phys. Chem. C* 123 (2019), pp. 2900–2910. DOI: 10.1021/acs.jpcc.8b10173.

[11] B. Hellsing and M. Persson. "Electronic Damping of Atomic and Molecular Vibrations at Metal Surfaces". In: *Phys Scr* 29 (1984), p. 360. DOI: 10.1088/0031-8949/29/4/014.

[12] M. Head-Gordon and J. C. Tully. “Molecular Dynamics with Electronic Frictions”. In: *J Chem Phys* 103 (1995), pp. 10137–10145. DOI: 10.1063/1.469915.

[13] J. I. Juaristi, M. Alducin, R. D. Muiño, H. F. Busnengo, and A. Salin. “Role of Electron-Hole Pair Excitations in the Dissociative Adsorption of Diatomic Molecules on Metal Surfaces”. In: *Phys. Rev. Lett.* 100 (2008), p. 116102. DOI: 10.1103/PhysRevLett.100.116102.

[14] M. J. Puska and R. M. Nieminen. “Atoms Embedded in an Electron Gas: Phase Shifts and Cross Sections”. In: *Phys. Rev. B* 27 (1983), p. 6121. DOI: 10.1103/PhysRevB.27.6121.

[15] J. I. Juaristi, M. Alducin, R. D. Muiño, H. F. Busnengo, and A. Salin. “Juaristi et al. Reply:” in: *Phys. Rev. Lett.* 102 (2009), p. 109602. DOI: 10.1103/PhysRevLett.102.109602.

[16] A. C. Luntz, I. Makkonen, M. Persson, S. Holloway, D. M. Bird, et al. “Comment on “Role of Electron-Hole Pair Excitations in the Dissociative Adsorption of Diatomic Molecules on Metal Surfaces”””. In: *Phys. Rev. Lett.* 102 (2009), p. 109601. DOI: 10.1103/PhysRevLett.102.109601.

[17] S. P. Rittmeyer, J. Meyer, J. I. Juaristi, and K. Reuter. “Electronic Friction-Based Vibrational Lifetimes of Molecular Adsorbates: Beyond the Independent-Atom Approximation”. In: *Phys. Rev. Lett.* 115 (2015), p. 046102. DOI: 10.1103/PhysRevLett.115.046102.

[18] O. Bünermann, H. Jiang, Y. Dorenkamp, A. Kandratsenka, S. M. Janke, et al. “Electron-Hole Pair Excitation Determines the Mechanism of Hydrogen Atom Adsorption”. In: *Science* 350 (2015), pp. 1346–1349. DOI: 10.1126/science.aad4972.

[19] R. J. Maurer, M. Askerka, V. S. Batista, and J. C. Tully. “Ab Initio Tensorial Electronic Friction for Molecules on Metal Surfaces: Nonadiabatic Vibrational Relaxation”. In: *Phys. Rev. B* 94 (2016), p. 115432. DOI: 10.1103/PhysRevB.94.115432.

[20] M. Askerka, R. J. Maurer, V. S. Batista, and J. C. Tully. “Role of Tensorial Electronic Friction in Energy Transfer at Metal Surfaces”. In: *Phys. Rev. Lett.* 116 (2016), p. 217601. DOI: 10.1103/PhysRevLett.116.217601.

[21] M. Askerka, R. J. Maurer, V. S. Batista, and J. C. Tully. “Erratum: Role of Tensorial Electronic Friction in Energy Transfer at Metal Surfaces [Phys. Rev. Lett. 116, 217601 (2016)]”. In: *Phys. Rev. Lett.* 119 (2017), p. 069901. DOI: 10.1103/PhysRevLett.119.069901.

[22] R. J. Maurer, B. Jiang, H. Guo, and J. C. Tully. "Mode Specific Electronic Friction in Dissociative Chemisorption on Metal Surfaces: H_2 on Ag(111)". In: *Phys. Rev. Lett.* 118 (2017), p. 256001. DOI: 10.1103/PhysRevLett.118.256001. arXiv: 1705.09753 [cond-mat.mtrl-sci].

[23] P. Spiering and J. Meyer. "Testing Electronic Friction Models: Vibrational De-Excitation in Scattering of H_2 and D_2 from Cu(111)". In: *J. Phys. Chem. Lett.* 9 (2018), pp. 1803–1808. DOI: 10.1021/acs.jpclett.7b03182.

[24] Y. Zhang, R. J. Maurer, H. Guo, and B. Jiang. "Hot-Electron Effects during Reactive Scattering of H_2 from Ag(111): The Interplay between Mode-Specific Electronic Friction and the Potential Energy Landscape". In: *Chem. Sci.* 10 (2019), pp. 1089–1097. DOI: 10.1039/C8SC03955K.

[25] D. Novko, M. Alducin, M. Blanco-Rey, and J. I. Juaristi. "Effects of Electronic Relaxation Processes on Vibrational Linewidths of Adsorbates on Surfaces: The Case of CO/Cu(100)". In: *Phys. Rev. B* 94 (2016). DOI: 10.1103/PhysRevB.94.224306.

[26] L. Diekhöner, L. Hornekær, H. Mortensen, E. Jensen, A. Baurichter, et al. "Indirect Evidence for Strong Nonadiabatic Coupling in N2 Associative Desorption from and Dissociative Adsorption on Ru(0001)". In: *J. Chem. Phys.* 117 (2002), pp. 5018–5030. DOI: 10.1063/1.1498476.

[27] H. Mortensen, E. Jensen, L. Diekhöner, A. Baurichter, A. C. Luntz, et al. "State Resolved Inelastic Scattering of N2 from Ru(0001)". In: *J. Chem. Phys.* 118 (2003), pp. 11200–11209. DOI: 10.1063/1.1575210.

[28] A. C. Luntz and M. Persson. "How Adiabatic Is Activated Adsorption/Associative Desorption?" In: *J. Chem. Phys.* 123 (2005), p. 074704. DOI: 10.1063/1.2000249.

[29] V. Smil. "Detonator of the Population Explosion". In: *Nature* 400 (1999), p. 415. DOI: 10.1038/22672.

[30] K. Shakouri, J. Behler, J. Meyer, and G.-J. Kroes. "Analysis of Energy Dissipation Channels in a Benchmark System of Activated Dissociation: N2 on Ru(0001)". In: *J. Phys. Chem. C* 122 (2018), pp. 23470–23480. DOI: 10.1021/acs.jpcc.8b06729.

[31] M. J. Murphy, J. F. Skelly, A. Hodgson, and B. Hammer. "Inverted Vibrational Distributions from N2 Recombination at Ru(001): Evidence for a Metastable Molecular Chemisorption Well". In: *J. Chem. Phys.* 110 (1999), pp. 6954–6962. DOI: 10.1063/1.478601.

[32] L. Diekhöner, H. Mortensen, A. Baurichter, and A. C. Luntz. "Laser Assisted Associative Desorption of N2 and CO from Ru(0001)". In: *J. Chem. Phys.* 115 (2001), pp. 3356–3373. DOI: 10.1063/1.1386810.

[33] C. Díaz, A. Perrier, and G. J. Kroes. "Associative Desorption of N2 from Ru(0 0 0 1): A Computational Study". In: *Chem. Phys. Lett.* 434 (2007), pp. 231–236. DOI: 10.1016/j.cplett.2006.12.016.

[34] K. Shakouri, J. Behler, J. Meyer, and G.-J. Kroes. "Accurate Neural Network Description of Surface Phonons in Reactive Gas–Surface Dynamics: N_2 + Ru(0001)". In: *J. Phys. Chem. Lett.* 8 (2017), pp. 2131–2136. DOI: 10.1021/acs.jpclett.7b00784.

[35] B. Hammer, L. B. Hansen, and J. K. Nørskov. "Improved Adsorption Energetics within Density-Functional Theory Using Revised Perdew-Burke-Ernzerhof Functionals". In: *Phys. Rev. B* 59 (1999), pp. 7413–7421. DOI: 10.1103/PhysRevB.59.7413.

[36] J. Behler, S. Lorenz, and K. Reuter. "Representing Molecule-Surface Interactions with Symmetry-Adapted Neural Networks". In: *J. Chem. Phys.* 127 (2007), p. 014705. DOI: 10.1063/1.2746232.

[37] C. Diaz, J. K. Vincent, G. P. Krishnamohan, R. A. Olsen, G. J. Kroes, et al. "Multidimensional Effects on Dissociation of N_2 on Ru(0001)". In: *Phys. Rev. Lett.* 96 (2006), p. 096102. DOI: 10.1103/PhysRevLett.96.096102.

[38] D. Novko, M. Blanco-Rey, M. Alducin, and J. I. Juaristi. "Surface Electron Density Models for Accurate *Ab Initio* Molecular Dynamics with Electronic Friction". In: *Phys. Rev. B* 93 (2016), p. 245435. DOI: 10.1103/PhysRevB.93.245435.

[39] D. A. Sivak, J. D. Chodera, and G. E. Crooks. "Time Step Rescaling Recovers Continuous-Time Dynamical Properties for Discrete-Time Langevin Integration of Nonequilibrium Systems". In: *J. Phys. Chem. B* 118 (2014), pp. 6466–6474. DOI: 10.1021/jp411770f.

[40] L. Verlet. "Computer "Experiments" on Classical Fluids. i. Thermodynamical Properties of Lennard-Jones Molecules". In: *Phys. Rev.* 159 (1967), p. 98. DOI: 10.1103/PhysRev.159.98.

[41] G. Bussi, D. Donadio, and M. Parrinello. "Canonical Sampling through Velocity Rescaling." In: *J. Chem. Phys.* 126 (2007), p. 014101. DOI: 10.1063/1.2408420.

[42] L. Diekhöner, H. Mortensen, A. Baurichter, E. Jensen, V. V. Petrunin, et al. "N2 Dissociative Adsorption on Ru(0001): The Role of Energy Loss". In: *J. Chem. Phys.* 115 (2001), pp. 9028–9035. DOI: 10.1063/1.1413746.

[43] C. Díaz, J. K. Vincent, G. P. Krishnamohan, R. A. Olsen, G. J. Kroes, et al. "Reactive and Nonreactive Scattering of N2 from Ru(0001): A Six-Dimensional Adiabatic Study". In: *J. Chem. Phys.* 125 (2006), p. 114706. DOI: 10.1063/1.2229197.

[44] D. Novko, M. Alducin, and J. I. Juaristi. "Electron-Mediated Phonon-Phonon Coupling Drives the Vibrational Relaxation of CO on Cu(100)". In: *Phys. Rev. Lett.* 120 (2018), p. 156804. DOI: 10.1103/PhysRevLett.120.156804.

[45] D. Novko, J. C. Tremblay, M. Alducin, and J. I. Juaristi. "Ultrafast Transient Dynamics of Adsorbates on Surfaces Deciphered: The Case of CO on Cu(100)". In: *Phys. Rev. Lett.* 122 (2019), p. 016806. DOI: 10.1103/PhysRevLett.122.016806.

[46] C. Díaz, E. Pijper, R. A. Olsen, H. F. Busnengo, D. J. Auerbach, et al. "Chemically Accurate Simulation of a Prototypical Surface Reaction: H2 Dissociation on Cu(111)". In: *Science* 326 (2009), pp. 832–834. DOI: 10.1126/science.1178722.

[47] F. Nattino, D. Migliorini, G.-J. Kroes, E. Dombrowski, E. A. High, et al. "Chemically Accurate Simulation of a Polyatomic Molecule-Metal Surface Reaction". In: *J. Phys. Chem. Lett.* 7 (2016), pp. 2402–2406. DOI: 10.1021/acs.jpclett.6b01022.

[48] S. Baroni, S. de Gironcoli, A. Dal Corso, and P. Giannozzi. "Phonons and Related Crystal Properties from Density-Functional Perturbation Theory". In: *Rev. Mod. Phys.* 73 (2001), pp. 515–562. DOI: 10.1103/RevModPhys.73.515.

[49] P. Giannozzi, S. Baroni, N. Bonini, M. Calandra, R. Car, et al. "QUANTUM ESPRESSO: A Modular and Open-Source Software Project for Quantum Simulations of Materials". In: *J Phys Condens Matter* 21 (2009), p. 395502. DOI: 10.1088/0953-8984/21/39/395502.

[50] M. A. L. Marques, M. J. T. Oliveira, and T. Burnus. "Libxc: A Library of Exchange and Correlation Functionals for Density Functional Theory". In: *Comput. Phys. Commun.* 183 (2012), pp. 2272–2281. DOI: 10.1016/j.cpc.2012.05.007.

[51] D. R. Hamann. "Optimized Norm-Conserving Vanderbilt Pseudopotentials". In: *Phys. Rev. B* 88 (2013), p. 085117. DOI: 10.1103/PhysRevB.88.085117.

[52] M. Schlipf and F. Gygi. "Optimization Algorithm for the Generation of ONCV Pseudopotentials". In: *Comput. Phys. Commun.* 196 (2015), pp. 36–44. DOI: 10.1016/j.cpc.2015.05.011.

[53] M. Abadi, A. Agarwal, P. Barham, E. Brevdo, Z. Chen, et al. "TensorFlow: Large-Scale Machine Learning on Heterogeneous Systems". In: (2015). Software available from tensorflow.org.

[54] S. Plimpton. "Fast Parallel Algorithms for Short-Range Molecular Dynamics". In: *J. Comput. Phys.* 117 (1995), pp. 1–19. DOI: 10.1006/jcph.1995.1039.

[55] J. Meyer. "Ab Initio Modeling of Energy Dissipation during Chemical Reactions at Transition Metal Surfaces". PhD thesis. Freie Universität Berlin, Freie Universität Berlin, Germany, 2012.

[56] I. Goikoetxea, J. Beltrán, J. Meyer, J. I. Juaristi, M. Alducin, et al. "Non-Adiabatic Effects during the Dissociative Adsorption of O_2 at Ag(111)? A First-Principles Divide and Conquer Study". In: *New J. Phys.* 14 (2012), p. 013050. DOI: 10.1088/1367-2630/14/1/013050.

[57] S. Manzhos and T. Carrington. "A Random-Sampling High Dimensional Model Representation Neural Network for Building Potential Energy Surfaces". In: *J. Chem. Phys.* 125 (2006), p. 084109. DOI: 10.1063/1.2336223.

[58] S. Manzhos, R. Dawes, and T. Carrington. "Neural Network-Based Approaches for Building High Dimensional and Quantum Dynamics-Friendly Potential Energy Surfaces". In: *Int. J. Quantum Chem.* 115 (2015), pp. 1012–1020. DOI: 10.1002/qua.24795.